Hindawi
Advances in Materials Science and Engineering
Volume 2019, Article ID 4530954, 16 pages
https://doi.org/10.1155/2019/4530954

Research Article

Deformation Caused by Dynamic Load and Support Requirements in a Deep Gob-Side Entry Rock Mass

Yandong Zhang,[1] Yongjie Yang,[1] and Changhua Zhuge[2]

[1]*College of Mining and Safety Engineering, Shandong University of Science and Technology, Qingdao 266590, China*
[2]*College of Chemical and Environmental Engineering, Shandong University of Science and Technology, Qingdao 266590, China*

Correspondence should be addressed to Yongjie Yang; yyj.6125@163.com

Received 5 November 2019; Accepted 9 December 2019; Published 24 December 2019

Academic Editor: Fernando Lusquiños

Gob-side entries in deep coal mines can be subjected to dynamic loading when driving along the goaf. The effects of this dynamic loading and improved ground support requirements are investigated in the Gaojiabao Coal Mine, China. Numerical modeling is first used to simulate the deformation characteristics of rock surrounding the gob-side entry under dynamic load with the original support design. Dynamic loading in this scenario causes continual deterioration in rock properties, and deformation accumulates as the number of dynamic loads increases. Therefore, the overall strength and rigidity of the bolt support design need improvement, especially in terms of using yielding bolts that assist in releasing unnecessary support loads. The deformation characteristics of the rock surrounding the gob-side entry are combined with the concept of coupled pressure support to provide an optimized bolt support design. The support effects of the optimized design are then also numerically simulated and compared with the original support design. Deformation in the optimized design is significantly reduced, and roadway control is improved. Finally, the optimized design is applied and measured in a gob-side entry excavation. The field test results show that the potential for loosening, deformation, and failure of the surrounding rock is effectively controlled.

1. Introduction

Deep mining [1] is characterized by high ground pressure, which strongly affects underground conditions in deep coal mines. Deep coal mines can also be influenced by the impact of dynamic loads, which can lead to rock burst conditions in rock surrounding gob-side entries [2–8]. This in turn creates difficulties in designing and implementing adequate ground support. In recent years, many new studies have been conducted on surrounding rock deformation mechanisms and support strategies in relation to dynamic loading [9]. Qi et al. [10] defined rock burst as the phenomenon in which deformation energy stored by coal and the rock mass around a mine shaft and stope is released violently. Cook [11] found that the surrounding rock support system in roadways in South African coal mines is out of balance and the rock mass fails as a result of increasing mining depth. In such cases, energy is released during the failure of the coal and rock mass, which exceeds the amount of energy consumed, leading to the production of ground stress. Other studies have examined rock fracture instability and rock burst, based on catastrophe theory [12, 13]. He et al. [14] established a layer crack plate model of rock burst in a roadway in accordance with previous research. Then, by examining the deformation characteristics of the surrounding rock support system subjected to dynamic loading, it was shown that bolt support of burst-prone rock should have a certain yielding capacity. The abilities of such bolt support have also been studied, the results of which relate to an improved design method involving energy measurements for rock burst in roadways [15] to preempt rock burst conditions. The propagation mode and attenuation characteristics of vibration energy caused by seismic waves underground have also been studied [16]. The study focused on energy and stiffness theory in the analysis of rock failure in a coal mine roadway under the combined action of dynamic and static loads. The above studies have examined the source of rock burst and roadway support [17, 18] in areas prone to such,

but the deformation mechanism of gob-side entry driving (i.e., the impact of dynamic loading) needs further study to provide theoretical guidance for surrounding rock control and support. At the same time, the ground influences and mechanisms of dynamic loading need to be verified.

This paper presents a study of the deformation mechanism in rock surrounding a gob-side entry subjected to dynamic loads [19] in the Gaojiabao Coal Mine. Designs of bolt support parameters for controlling the surrounding rock along the goaf in this deep mine are also presented.

2. Engineering Background

Gaojiabao Coal Mine is located in Binchang Mining Area, Shanxi Province, China. The mining depth is >1000 m, the average thickness of the coal seam is 11.77 m, and the seam dips at 5°. The mine is subject to high in situ stresses. The southern part of the 103 and 101 working faces is mined completely, and the distance between the 103 working face and 101 goaf is 8 m. A downhole position schematic diagram of the working face and goaf layout is shown in Figure 1. Gob-side entry roadways can be affected by mining at the last working face because of the large burial depth and ineffective support. During roadway excavation, there is obvious deformation of the surrounding rock, bolt breakage, bending deformation, and failure of steel strips [20], amongst other support issues. The main coal seam #4 has a strong tendency to burst, and the overlying strata undergo fracturing. Under the combined action of impact dynamic load and mining stress, the deformation of surrounding rock can become severe and the support requirements will increase.

As the intensity of coal mining increases, shallow coal seam mining is decreasing, and more mines are entering deeper parts of their respective rock mass. As such, more rock bursts [21, 22] are expected in such mines, and the additional dynamic loading can lead to technical problems related to accumulation of deformation along gob-side entry roadways. Therefore, it is important to study the damage degradation and deformation failure mechanisms in rock surrounding the gob-side entry under dynamic loading. As such, the design of bolt patterns and parameters for the gob-side entry has important theoretical and practical significance for support design in deep coal mines under these conditions.

3. Numerical Simulation of Surrounding Rock Deformation

FLAC3D software uses finite element modeling to simulate the mechanical behavior of soil, rock, and other materials. It can accurately demonstrate the process of material yield, plastic flow, softening, and failure. FLAC3D was used in this study to simulate conditions of the 103 gob-side entry roadway at Gaojiabao Mine under dynamic loading. The deformation and failure mechanism of the surrounding rock was also studied, providing a theoretical basis and support for the determination of support design.

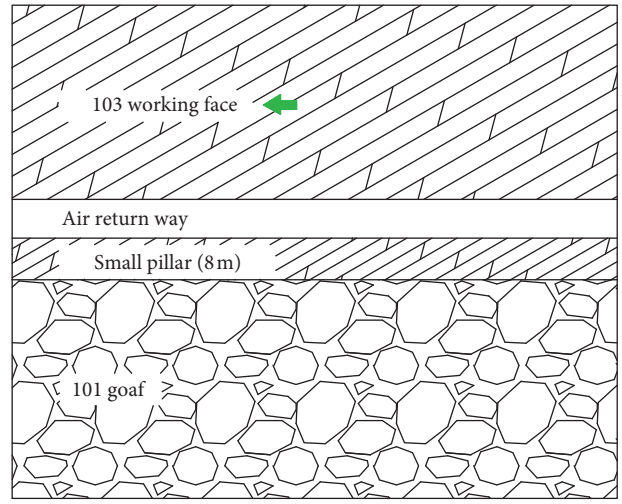

Figure 1: Schematic representation of a working face in the Gaojiabao coal mine.

3.1. Establishment of Numerical Model. The three-dimensional numerical calculation model of the 103 gob-side entry was established in FLAC3D 5.0 (Itasca Consulting Group, Inc., USA) using a model of 300 × 140 × 60 m. The roadway length was set at 100 m, the width at 5 m, and the height at 3.5 m. The left goaf of the roadway is arranged in 3D (X, Y, Z) with values in the range of −100–0 m (X), 20–120 m (Y), and 0–6 m (Z). According to the conversion relationship between bulk density and density, combined with the parameters in Table 1, the vertical stress is 22 MPa.

The X and Y directions of the model are constrained by horizontal displacement, the bottom boundary is constrained by vertical displacement, the top of the model is a free boundary, and the upper boundary is loaded at 22 MPa. A horizontal stratification model is adopted because of the low dip angle of the coal seam. The stratification is, from bottom to top, aluminous mudstone, mudstone, coal seam, mudstone, and fine sandstone.

3.2. Numerical Simulation of Deformation under Dynamic Load. Mines subjected to dynamic loading, such as overlying high-level strata fracturing, can frequently experience rock burst and other dynamic phenomena. Roadways are constantly subjected to impact loading during the service period of the roadway, resulting in the surrounding rock experiencing multiple dynamic loads. Therefore, the deformation caused by multiple dynamic loads can be simulated and calculated but is limited in terms of simulation time and workload. This paper only simulates the deformation of surrounding rock under finite dynamic loads. The existing technical means and observation conditions cannot completely describe the dynamic load situation in the mine because of the complexity of the actual mine and the frequent vibrations that occur. The model is simplified by making use of the theoretical simple harmonic wave in simulating the dynamic load impact in the mine. The equation of the vibration wave is as follows:

Table 1: Lithologies and petrophysical parameters of the roof and floor.

Lithology	ρ (kg/m^3)	K (MPa)	G (MPa)	C (MPa)	Rm (MPa)	φ (°)
Fine sandstone	2460	7500	8300	4.25	4.84	29
Mudstone	2000	5400	3900	3.56	3.05	24
Coal seam	1500	620	820	0.63	0.3	31
Al mudstone	2000	3000	3900	3.56	3.05	24
Mudstone	2400	8700	9030	6.65	4.53	30

ρ is density, K is bulk modulus, G is shear modulus, C is cohesion, Rm is tensile strength, and φ is friction angle.

$$\text{wave} = A \sin 2.0 \times \pi \times \text{frep} \times \text{dytime}, \quad (1)$$

where A is the amplitude, frep is the frequency, and dytime is the calculation time. In the simulation, the dynamic load impact is applied on the upper part of the modeled coal seam. After the first dynamic load calculation is completed, the dynamic load is applied again at the same position for the second calculation. The objective conditions and simulation time are limited, meaning that the calculation times cannot be repeated indefinitely. Here, only 10 dynamic load calculations are carried out for roadways to reflect the cumulative deformation [23, 24] and variation trend in the rock surrounding the roadways. Four monitoring points were arranged: at the roof, the floor, and at the two sides of the roadway (Figure 2).

A monitoring surface was set every 5 m over the range of 20–120 m in the Y-direction to record and analyze the displacement and deformation velocity in the surrounding rock. A large amount of data were generated, and as such only the simulation results of displacement and deformation velocity after 1, 6, and 10 dynamic loads are analyzed here.

3.2.1. Characteristics of the Plastic Zone during Dynamic Loading. The plastic zone of the surrounding rock after one, six, and ten dynamic load impacts was analyzed, as shown in Figures 3 and 4.

From Figures 3 and 4, it can be seen that the plastic zone increases gradually with an increase in the number of dynamic loads. However, this trend decreases after the sixth dynamic load. The plastic zone on the side of a small roadway pillar is larger than that of the roof, floor, and coal seam. It can be expected that, under the frequent impact of dynamic loads, the plastic zone will gradually become larger, and the mechanical performance of the rock will continue to deteriorate, resulting in gradually increasing deformation that could potentially lead to complete failure.

3.2.2. Displacement Response of Surrounding Rock. Displacement response diagrams for the surrounding rock under dynamic loading are shown in Figures 5–7. These diagrams show that, in the initial stage of dynamic load calculation, the displacement of the roadway oscillates but gradually oscillates less over time.

Table 2 presents displacement monitoring data from the roadway after one, six, and ten dynamic loads. The data show that displacement increases with increasing dynamic loads in both the X- and Z-directions. The displacement and deformation of the monitoring point on the left side of the small coal pillar are the largest, likely because it is affected by two working faces. As such, the small pillar side is a key point of support in gob-side entry roadways in deep coal mines.

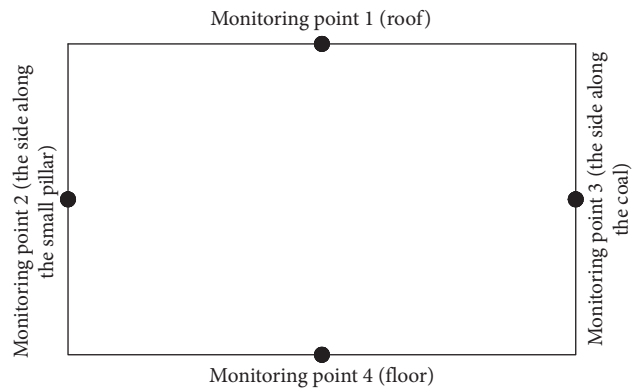

Figure 2: Schematic cross section showing the layout of monitoring points in the rock surrounding the roadway.

Figure 5 shows that deformation in the surrounding rock increases during the initial stage of dynamic loading in the X-direction but decreases after six dynamic loads. Displacement in the Z-direction is uncontrolled under multiple dynamic loads, showing a strongly oscillatory trend. This indicates that the roadway roof and floor may be damaged after multiple dynamic loads. For example, after simulation of three dynamic loads, it was found that the fluctuation in Z-direction displacement was strongly oscillatory, suggesting that the roadway roof and floor could be destroyed after only three dynamic loads.

Frequent dynamic loading of the mine results in a gradual increase in deformation of the roadway surrounding rock, and total deformation is significant. If the strength and stiffness of the bolt support system are insufficient, or the allowable deformation of the support system is too small, then continued dynamic load impacts will result in the roadway support system becoming ineffective or potentially destroyed.

3.2.3. Deformation Velocity Response. When simulating the impacts of dynamic loading of the roadway, the deformation law and characteristics can be analyzed in terms of the vibration deformation speed of monitoring points subjected to the dynamic loads. The simulation results of deformation velocity response at monitoring points after 1, 6, and 10 dynamic loads are shown in Figures 8–10.

From Figure 10, it can be seen that the deformation speed of each monitoring point is intense under several

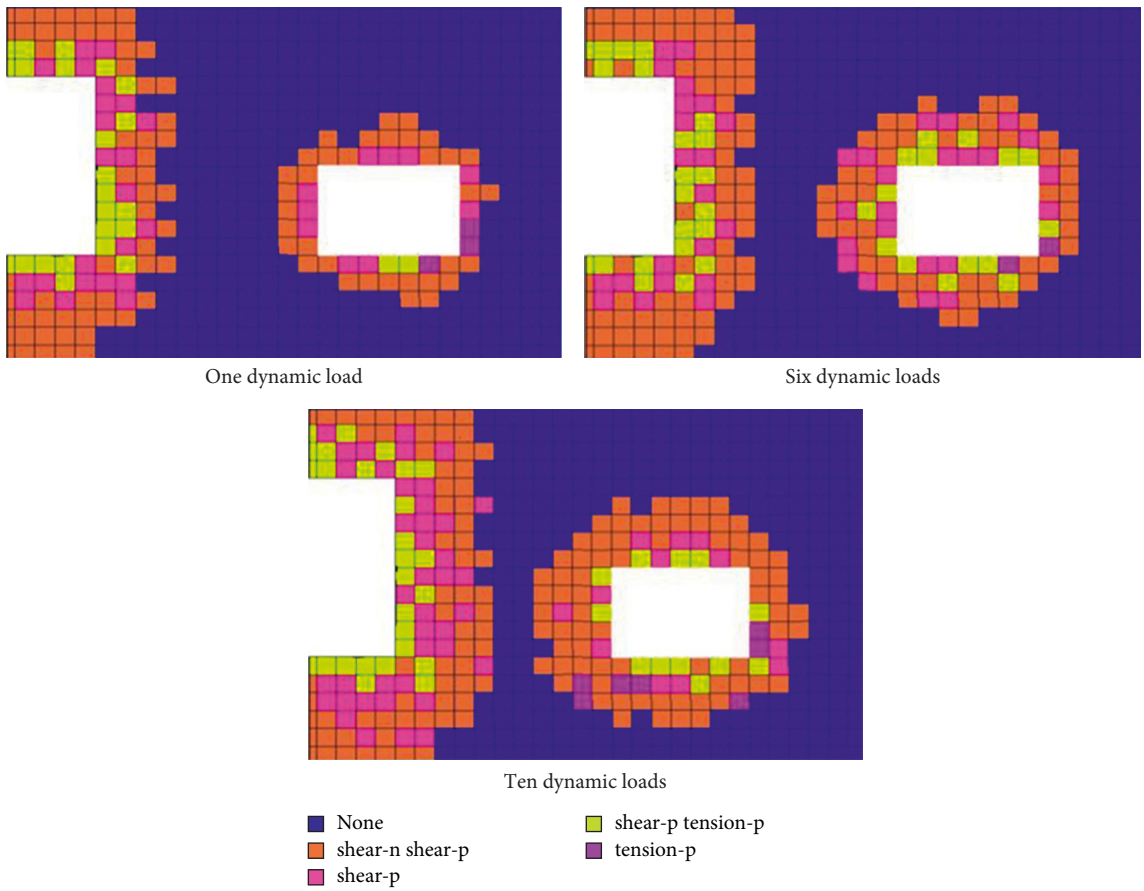

Figure 3: FLAC simulations of the plastic zone after one, six, and ten dynamic loads.

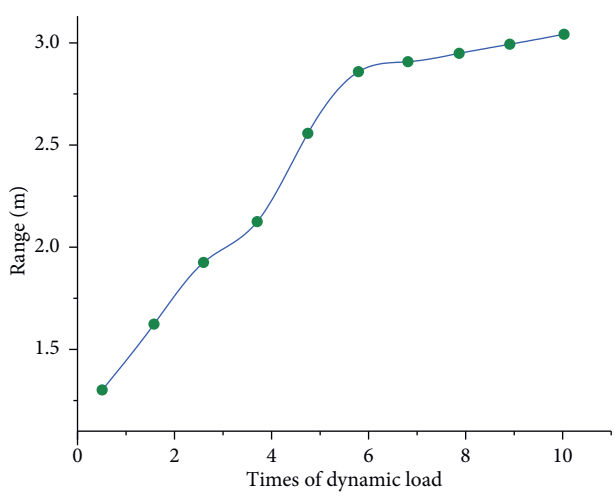

Figure 4: Curve showing the increasing range of plastic zone on the side of a small pillar relative to multiple dynamic loads.

initial dynamic loads, followed by a gradual decrease over time. However, because the roadway will undergo multiple dynamic loads during the service period, deformation of the surrounding rock (i.e., the plastic zone) will gradually shift to greater depths. It is expected that such deformation of the roadway along a goaf will accumulate continuously, and the total deformation will be significant. Therefore, the support design of a roadway along a goaf in a deep mine, such as the Gaojiabao Coal Mine, requires an increase in the overall stiffness and strength of the bolt support system to prevent excessive deformation. It is also required that the flexibility of the bolt support system is increased by using yielding bolts and yielding cable anchors [25]. Such a bolt support system will not only ensure high support strength and stiffness but also allow for deformation to occur without compromising the anchors. This support system will therefore be adapted to the actual situation of large deformation in rocks surrounding deep mine gob-side entries subjected to dynamic loads and ensure effective stability.

4. Support of Rock Surrounding the Gob-Side Entry

In view of the characteristics of large-scale damage of the surrounding rock and the severe deformation in rock surrounding the gob-side entry, it is necessary to adopt the overall balanced support method of high strength, high stiffness, and yield capacity. In other words, the support design is based on the concept of integrated coupling and equalizing pressure support [26].

4.1. Integrated Coupling of High Strength Yielding Roadway Support. Coupled equalizing pressure support refers to the

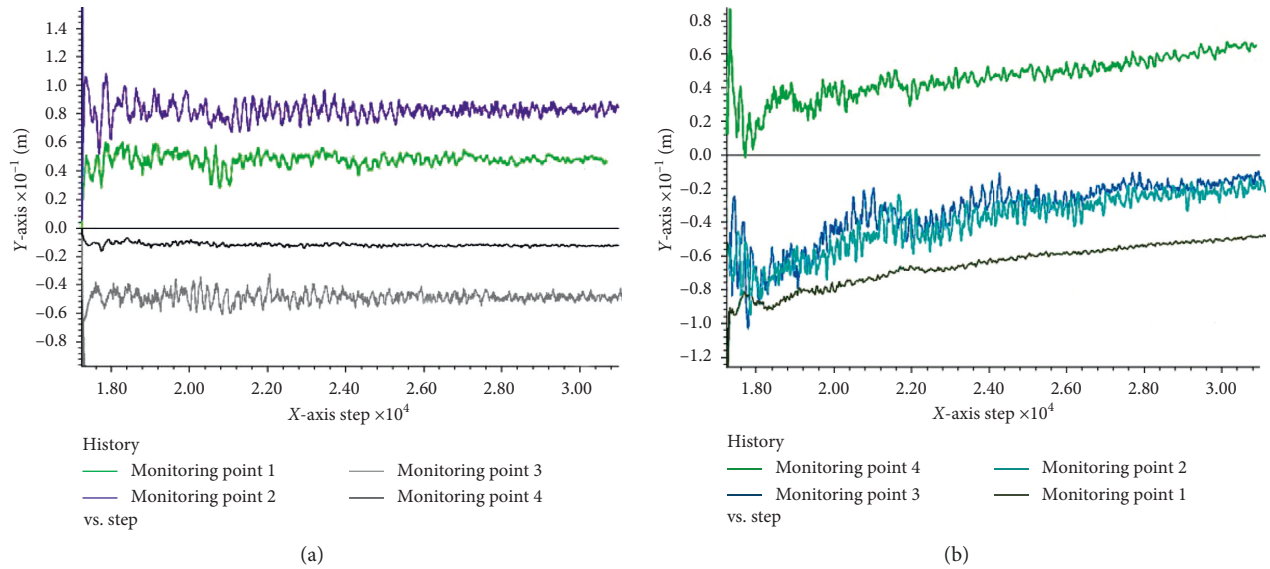

Figure 5: Displacement response diagrams after one dynamic load. (a) X-direction displacement and (b) Z-direction displacement.

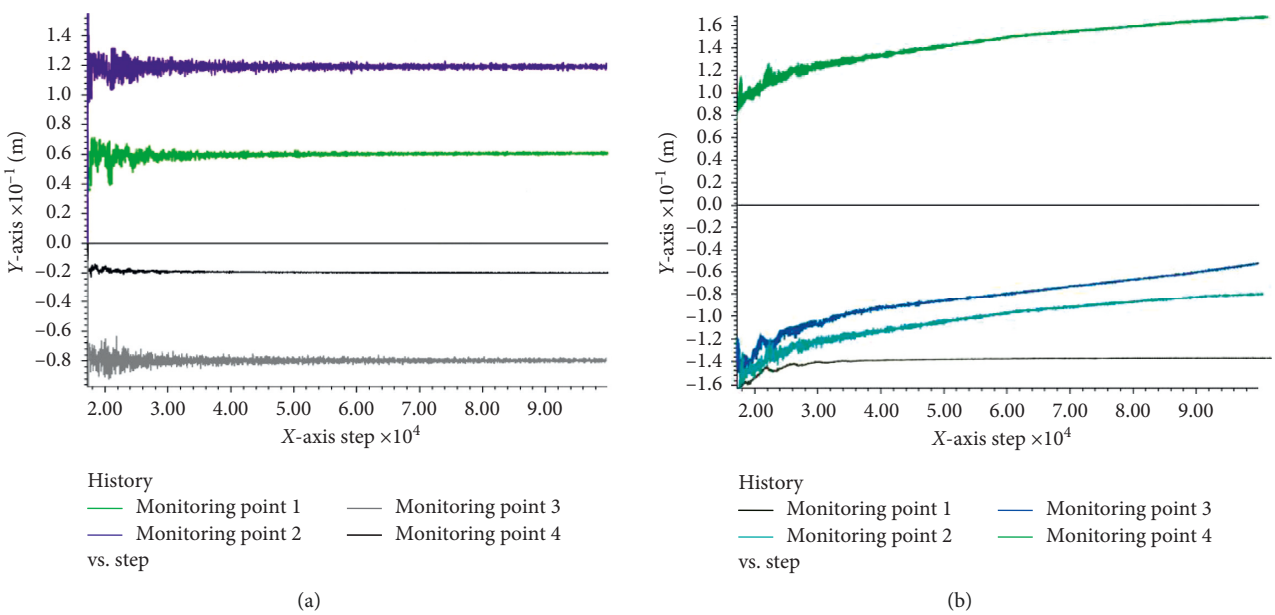

Figure 6: Displacement response diagrams after six dynamic loads. (a) X-direction displacement and (b) Z-direction displacement.

coupling between individual support elements and surrounding rock and coupling amongst all support elements. As such, the various aspects of coupling are summarized as follows:

(1) Coupling between bolts and surrounding rock: the support strength and deformation performance of the bolt support system must be coupled with the surrounding rock to achieve stability

(2) Coupling between the cable anchor system and surrounding rock: the load bearing and deformation performance of the cable anchor system must be coupled with the surrounding rock to achieve stability

(3) Coupling between bolts: displacement and stresses are known to vary amongst the roof, floor, and sides of the roadway, which results in differences in the forces applied to the bolts in different positions. This could potentially result in sequential bolt failure as highly stressed bolts may fail first, thus transferring stresses to adjacent bolts

(4) Coupling between bolts and cable anchors: deformation coupling between bolts and cable anchors is very important. There are differences in the physical and mechanical properties and geometric dimensions between bolts and cable anchors. If the difference is inappropriate after design and

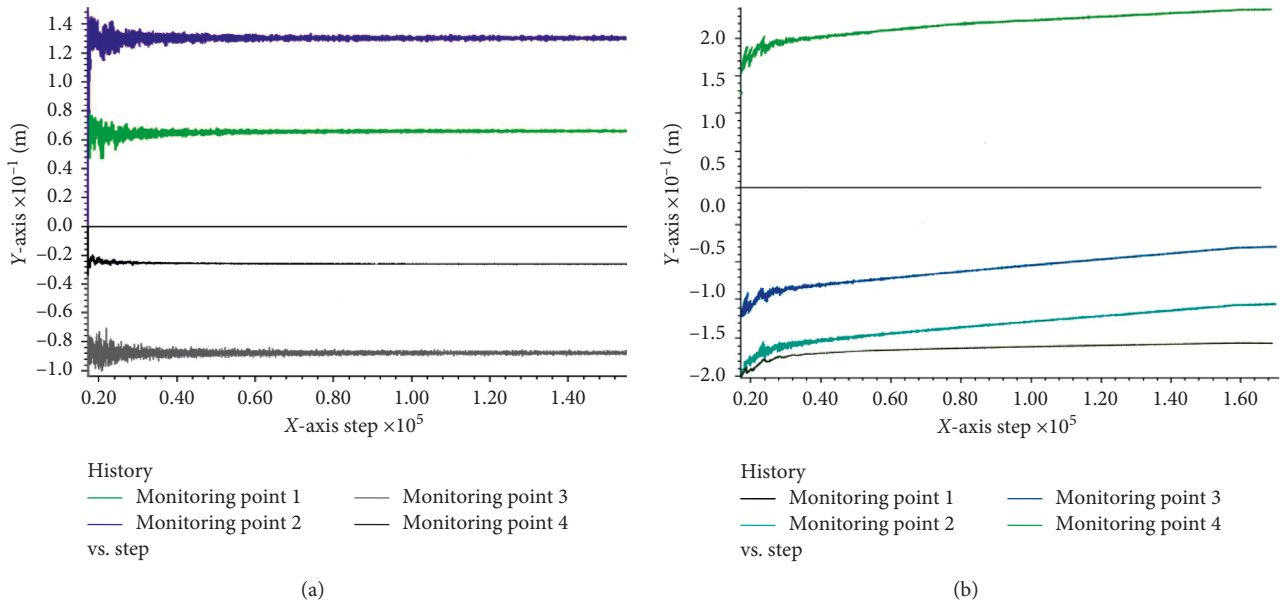

Figure 7: Displacement response diagrams after ten dynamic loads. (a) X-direction displacement and (b) Z-direction displacement.

Table 2: Displacement monitoring result record.

Monitoring point number times of dynamic load	X-direction displacement (mm)			Z-direction displacement (mm)		
	One	Six	Ten	One	Six	Ten
1	48.8	60.6	63.8	−48.0	−142.0	−210.0
2	85.0	120	130.9	−21.0	−79.0	−151.0
3	−50.0	−79.0	−86.0	−15.0	−48.0	−80.0
4	−10.0	−20.0	−25.2	64.0	168.0	240.0

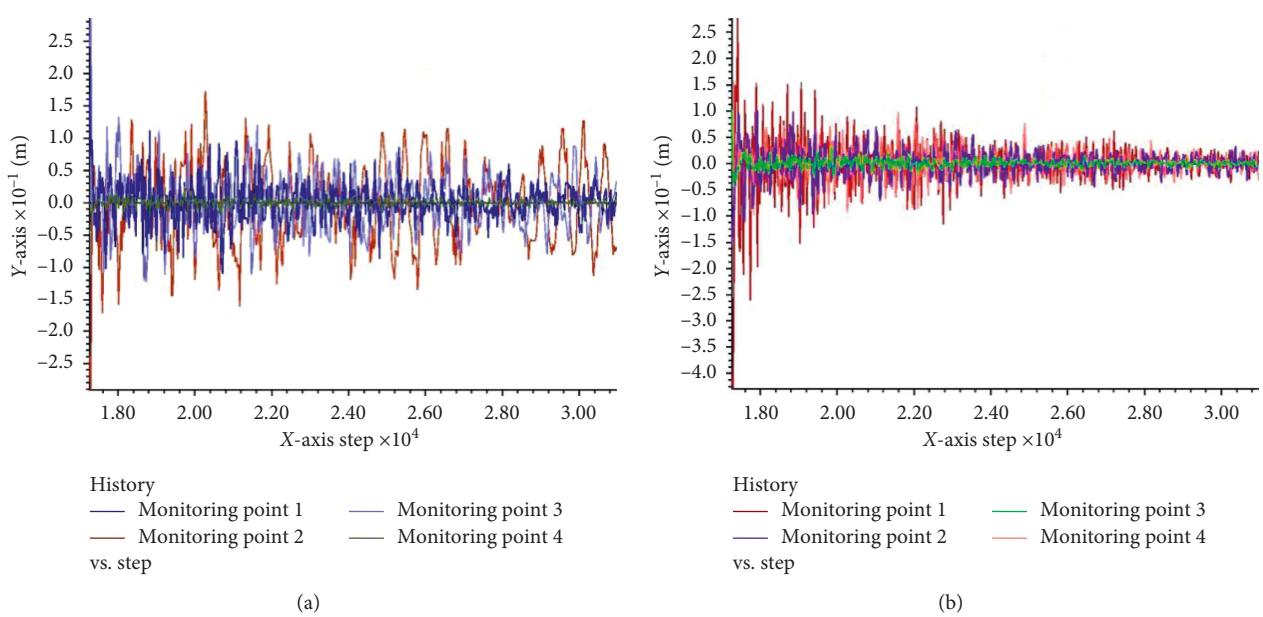

Figure 8: Deformation velocity response diagrams for one dynamic load. (a) X-directional deformation velocity and (b) Z-directional deformation velocity.

implementation, it can affect the degree of support offered to the surrounding rock and the nature of its deformation

(5) To prevent "uncontrollable" deformation, high-strength and high-stiffness support systems must have some yielding capacity. However, this yielding

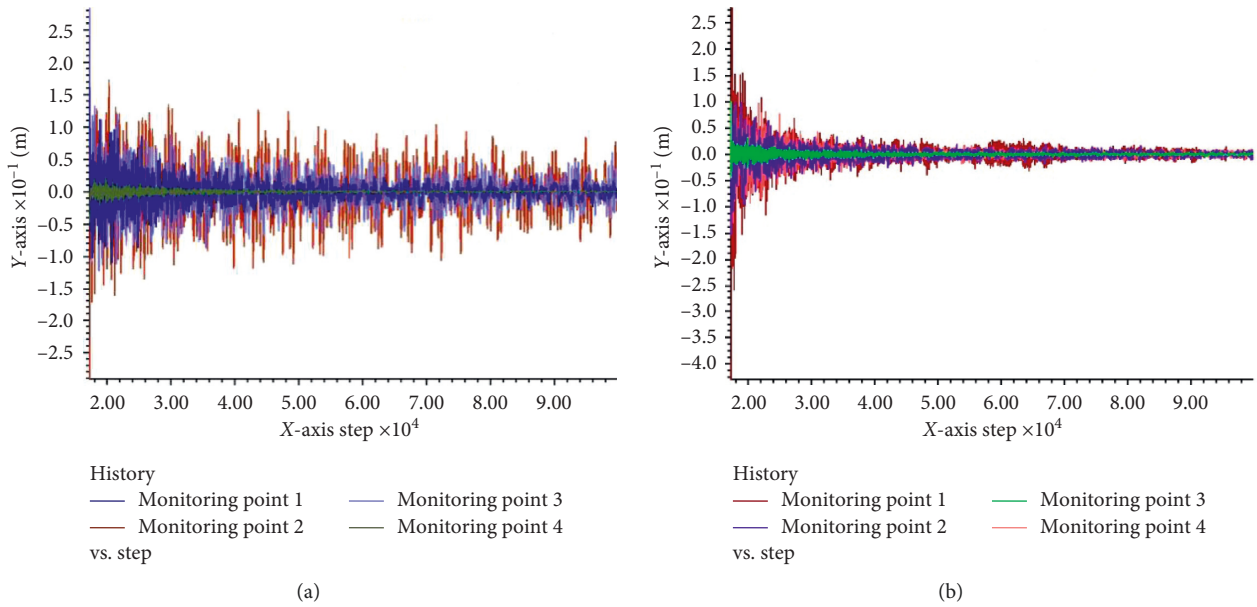

Figure 9: Deformation velocity response diagrams for six dynamic loads. (a) X-directional deformation velocity and (b) Z-directional deformation velocity.

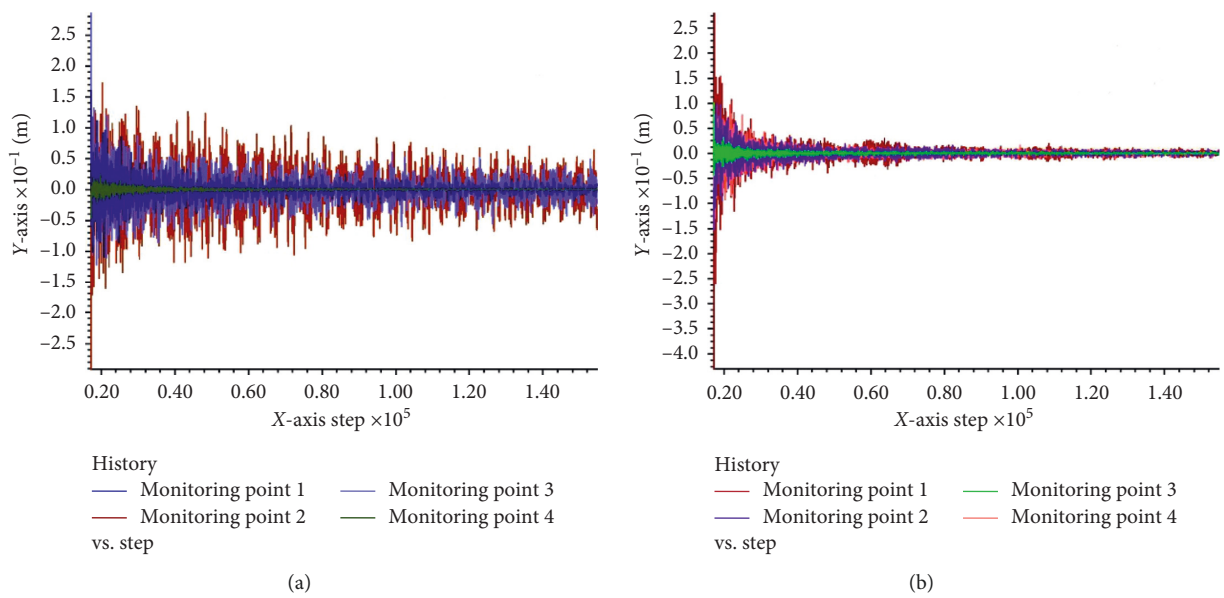

Figure 10: Deformation velocity response diagrams for ten dynamic loads. (a) X-directional deformation velocity and (b) Z-directional deformation velocity.

must be controlled so that the support system slowly yields under higher support strength rather than being allowed to freely yield (uncontrolled)

4.2. Parameter Optimization of Bolt Support. After implementation of the original support scheme, some problems developed, such as low pretensioning forces applied to the bolts and cable anchors, low resistance of the bolts and cable anchors, and decoupling between the support offered by the bolts and cable anchors. This affected the roadway support. The bolt support design [27] of the gob-side entry at the 103 working face was carried out using the integrated coupling concept and took into account the length, pretensioning force, yield strength, elongation, and row spacing of bolts and cable anchors. Bolt lengths were designed to be 2.8 m based on the intended life-of-mine and the influences of mining processes. The impact of rock burst required that high-strength threaded steel with energy absorption capacity be used for bolts. In instances where the lengths of bolts were increased, the lengths of cable anchors were matched appropriately to achieve mutual coordination. The pretensioning force applied to each bolt was set at no less than 5 t. It should be noted that the yield point of the high-

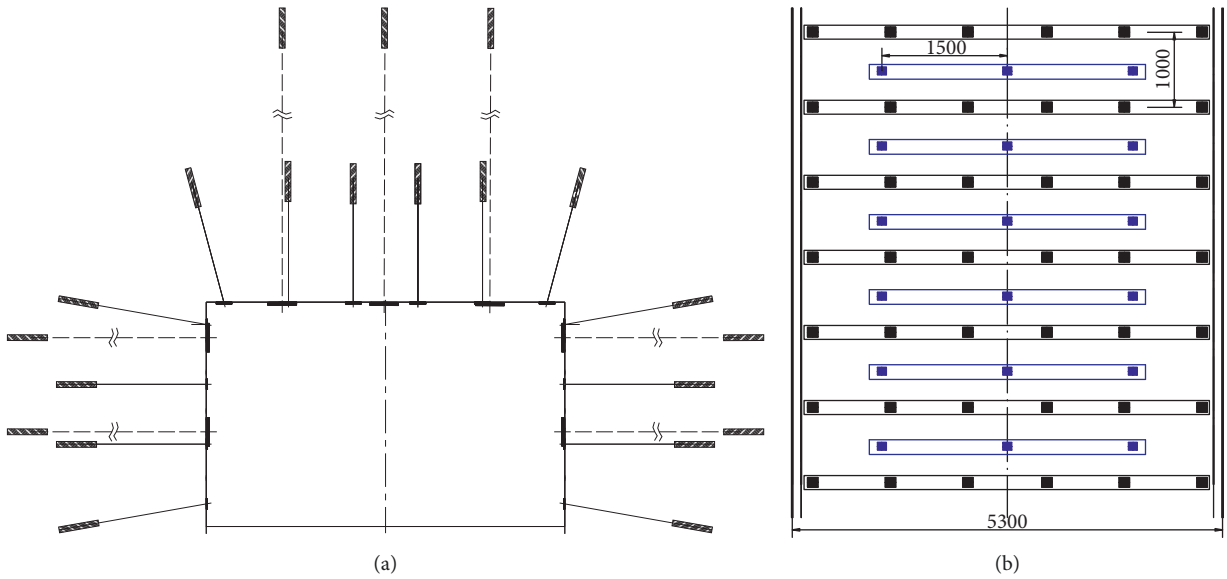

Figure 11: Sketch of air return way.

strength yielding bolt is 17 t and the maximum range of elastic yield is 30 mm. The yield strength of the bolt body must be greater than 200 kN, and the maximum tensile strength of the bolt must exceed 240 kN. The specific optimization scheme is described below in five steps and is illustrated in Figure 11.

(1) Roof: high-strength torsional stress yielding bolts were adopted for the roof. The bolt body is Q500 high-strength screw steel, 2800 mm in length, with a row spacing between bolts of 1000 × 1000 mm (each row contains 6 bolts). The anchor plates are high-strength spherical plates (150 × 150 × 10 mm) with a bearing capacity of >33 t. The roof surface was clad with a combination of weld mesh and W-shaped steel strips

(2) Sidewalls: high-strength snake-shaped pressure-relieving bolts were adopted for both sidewalls. The bolt body is Q500 high-strength screw steel, 2800 mm in length, with a row spacing between bolts of 1000 × 1000 mm (each row contains 4 bolts). The anchor plates are high-strength spherical plates (150 × 150 × 10 mm). The sidewall surfaces were also clad with a combination of weld mesh and W-shaped steel strips

(3) Roof cable anchors: for small coal pillar gob-side entries, 6500–8000 mm long steel strand was selected to maximize cable length but not result in insertion into the mudstone of the roof. This selection also took site geological conditions into account. Cable anchor lengths in the normal section of 7000 mm (21.8 mm diameter) were selected, with pretensioning forces of no less than 15 t. The row spacing between anchors was set at 1000 × 1500 mm

(4) Cable anchor parameters: cable anchor lengths of 4500 mm were selected, with a diameter of 18.9 mm and row spacing between anchors of 1000 × 1500 mm. Pretensioning forces of no less than 10 t were applied

(5) Surface support: a combination of bidirectional tensile plastic mesh and W-shaped steel strips was used, along with grouting for the side surface of the small coal pillar

4.3. Numerical Simulation of Surrounding Rock Control Effects on Optimized Support Plan

4.3.1. Simulation Scheme. Simulations were undertaken in accordance with the model presented in Section 3.2. The vibration wave equation and the loading position were not changed, but the roadway supporting parameters were. Then, dynamic loads under the optimized supporting scheme were simulated many times, and comparisons between the original support and the optimized support were analyzed.

4.3.2. Displacement and Deformation Characteristics under Optimized Support Scheme. Ten iterations of dynamic loading of the gob-side entry driving were simulated with the optimized support scheme implemented. Note that the layout of monitoring points is the same as discussed in Section 3.2. Only the results from one, six, and ten dynamic loads are listed because of the large amount of data collected.

Displacement response data, for both original support design and simulated under optimized conditions, are summarized in Tables 3 and 4. In terms of displacement response in the surrounding rock, it can be seen that, while the number of dynamic loads increases, there is a clear difference in the deformation of surrounding rock for the two designs (Figures 12–14). The differences are evident in both the vertical (Z) and horizontal (X) displacements.

The deformation of surrounding rock under each dynamic load in the original support scheme is clearly larger

Table 3: X-direction displacements for one, six, and ten dynamic loads.

Monitoring point number times of dynamic load	X-direction displacement under the original supporting scheme (mm)			X-direction displacement under optimized supporting scheme (mm)		
	One	Six	Ten	One	Six	Ten
1	48.8	60.6	63.8	21.4	35.6	36.2
2	85.0	120.0	130.9	43.0	80.7	86.0
3	−50.0	−79.0	−86.0	−15.0	−30.0	−33.2
4	−10.0	−20.0	−25.2	−8	−15	−18

Table 4: Z-direction displacements for one, six, and ten dynamic loads.

Monitoring point number times of dynamic load	Z-direction displacement under the original supporting scheme (mm)			Z-direction displacement under optimized supporting scheme (mm)		
	One	Six	Ten	One	Six	Ten
1	−48	−142	−210.0	−15.8	−84.5	−111.0
2	−21	−79	−151.0	−5.0	−36.2	−63.2
3	−15	−48	−80.0	−4.7	−25.5	−31.2
4	64.0	168	240.0	44	118	136.9

than that when the optimized support scheme is implemented. Deformation under the original support scheme is also greater at each of the loading steps (1, 6, and 10). Variation in deformation is also larger than that in the optimized scheme, and overall deformation also increases. Under the original support scheme, it is evident that the surrounding rock properties deteriorate after multiple dynamic loads. After adopting the optimized scheme, the bearing capacity of surrounding rock is effectively improved.

Velocity response data (Figures 15–17) show that the deformation speed in the roadway under the optimized support scheme is less than that under the original support scheme. This is true after multiple dynamic loads, in both horizontal and vertical directions. The optimized support scheme effectively controls deformation of the roadway and the surrounding rock.

5. Analysis of Support Effects in the Gob-Side Entry

By analyzing the maintenance status of the roadway entry bolts located along the 103 working face goaf, it was possible to quantify the deformation in the rock surrounding the roadway after implementing the optimized support scheme. It was then possible to analyze the support performance of the cable anchors and evaluate the support effect relative to timing of installation. The adaptability of the bolt support parameters and support strength provided to the surrounding rock along the goaf was analyzed from underground stress monitoring data. From this, it is possible to provide the scientific basis for further optimization of the roadway support design.

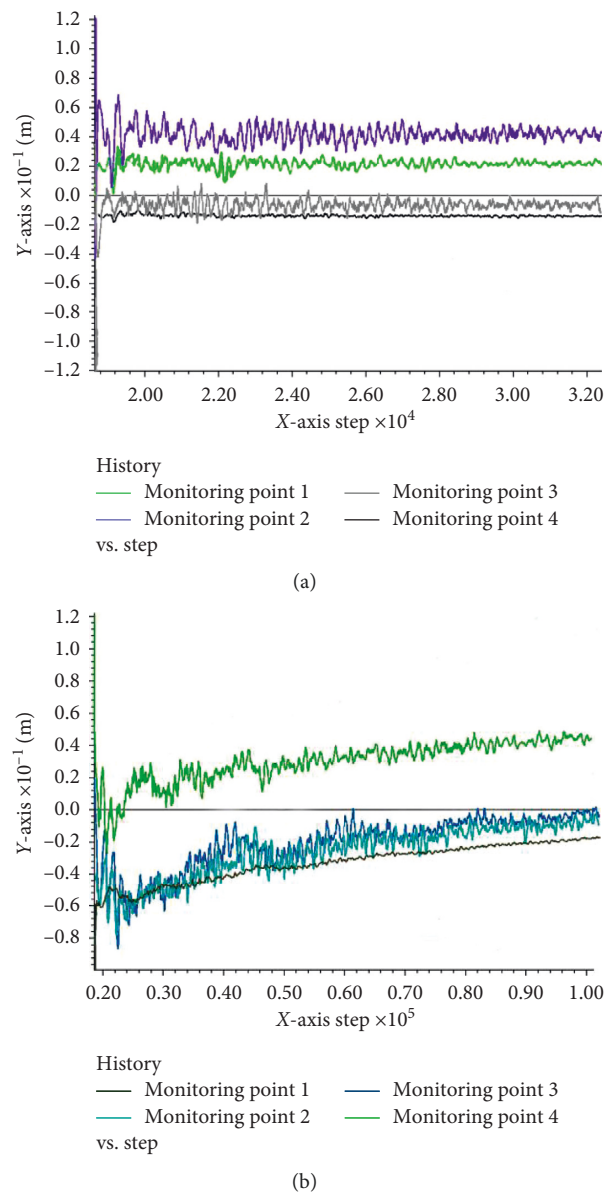

Figure 12: Displacement response diagram for one dynamic load. (a) X-direction displacement and (b) Z-direction displacement.

5.1. Stress Monitoring Scheme. Systematic monitoring of underground stress during driving and mining in the gob-side roadway was achieved using three stations in the air return way. Monitoring of pretensioning forces and working resistance of bolts and cable anchors was also undertaken, as well as monitoring of rock deformation (surface displacement of the coal-rock mass).

Station #1 is located 90–130 m along the coal from the 103 working face open-off cut. Station #2 is located ~230 m from the 103 working face cutting hole (along a goaf) and station #3 is located ~300 m from the 103 working face cutting hole (along a goaf). The layout of the stations is shown in Figure 18.

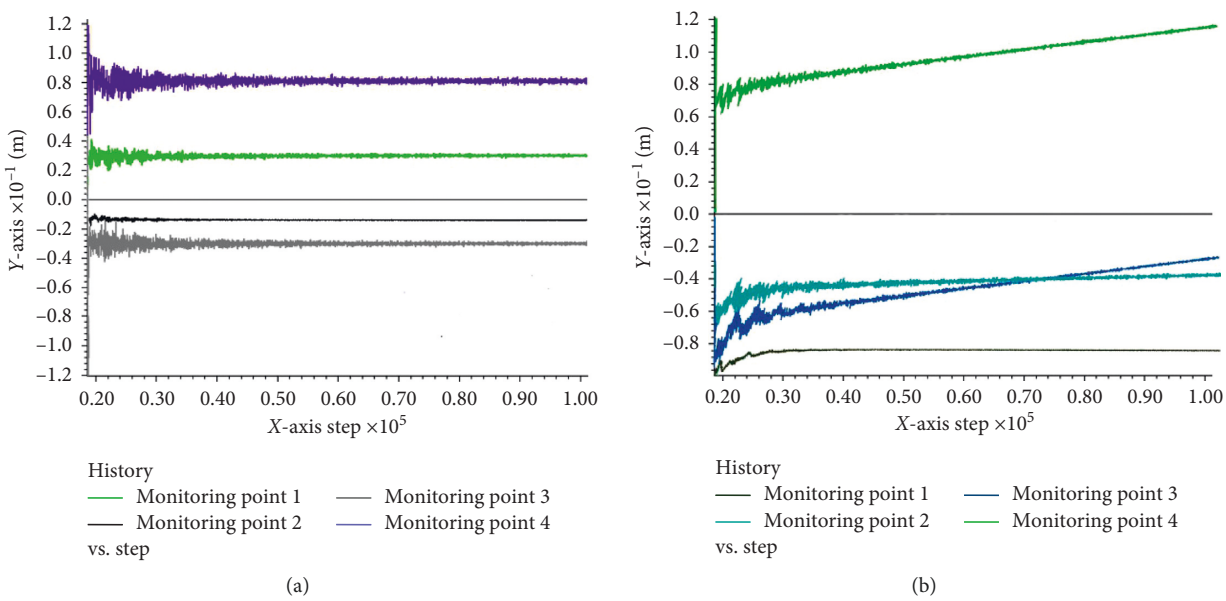

Figure 13: Displacement response diagram for six dynamic loads. (a) X-direction displacement and (b) Z-direction displacement.

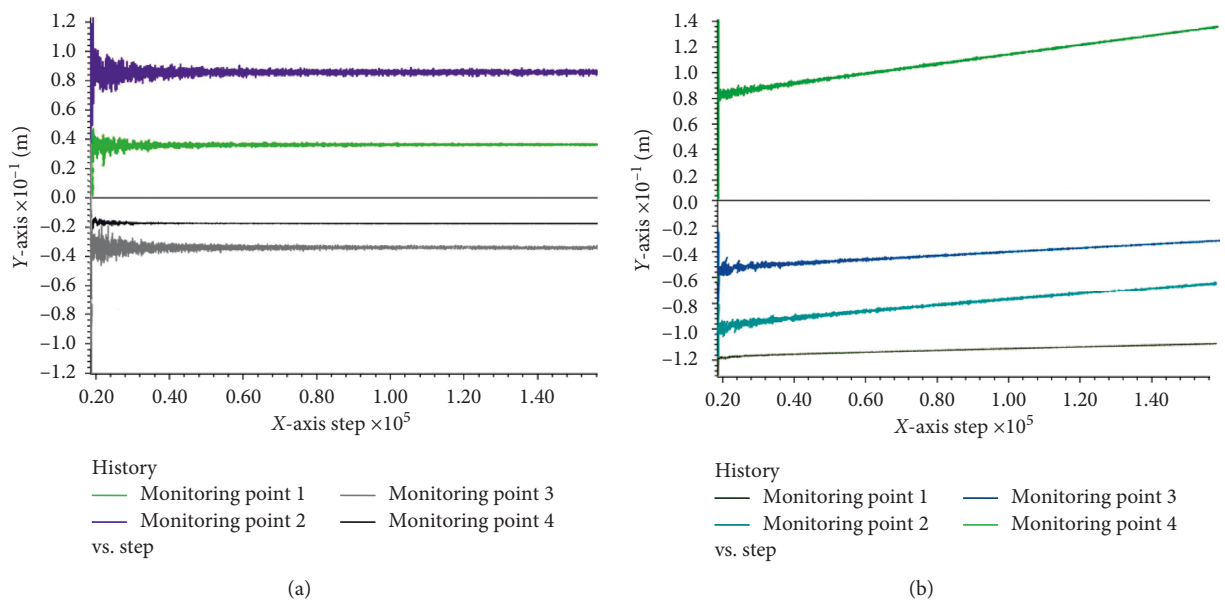

Figure 14: Displacement response diagram for ten dynamic loads. (a) X-direction displacement and (b) Z-direction displacement.

5.2. Analysis of Monitoring Results. Three stations were arranged in the roadway to monitor multiple bolts and cable anchors. Only a small selection of monitoring data and analyses are presented because of the large number of dynamometers monitored. These monitoring data are shown in Figure 19.

The monitoring data reveal that the pretensioning force of the initial bolt is highest overall, with a maximum of 9.69 t, minimum of 1.53 t, and average of 5 t. This equates to 20.83% of its tensile strength. The pretensioning force of the initial installation of the cable anchor is also highest overall, with a maximum of 14.28 t, minimum of 6.63 t, and average of 11.48 t. This equates to 22.96% of its tensile strength. The higher pretensioning force increases the overall rigidity of the rock stratum in the anchorage range, effectively restraining harmful deformation in the shallow surrounding rock in time. This prevents the deepening of broken surrounding rock, thus improving the self-supporting ability of the rock.

Once the roadway is stabilized, the working resistance of bolts is generally 6–11 t, with an average of 8.96 t, which is 37.33% of the tensile strength of the cable anchors. The working resistance of the cable anchors is generally 14–20 t, with an average of 14.62 t, which is 29.24% of the tensile

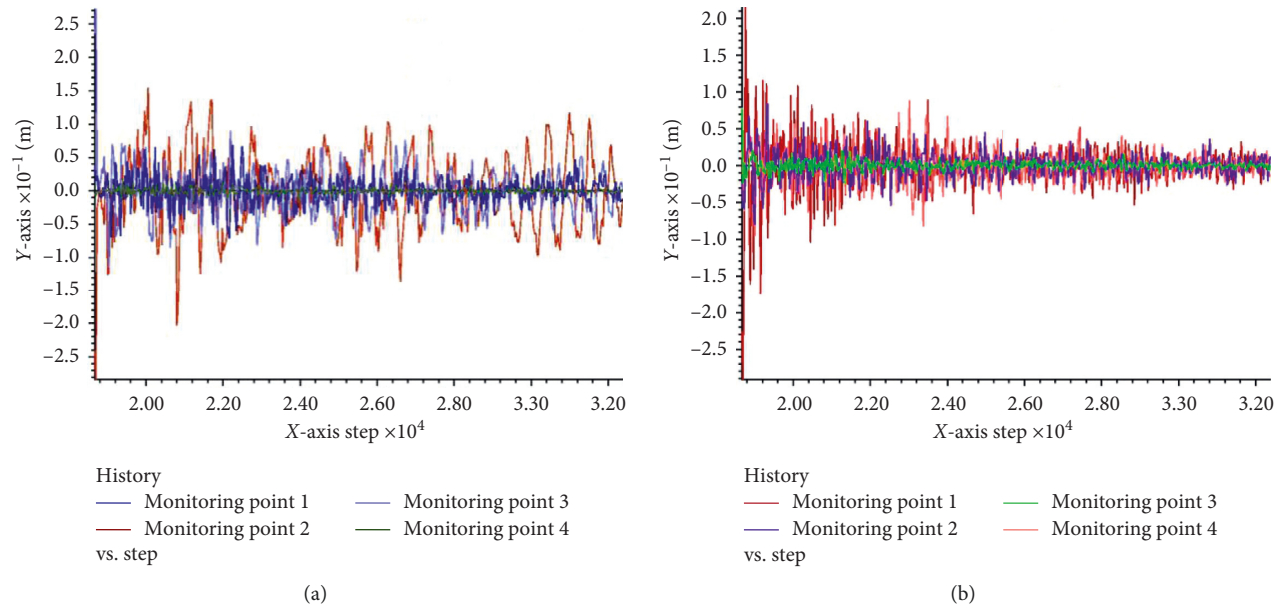

Figure 15: Velocity response diagram for one dynamic load. (a) X-directional deformation velocity and (b) Z-directional deformation velocity.

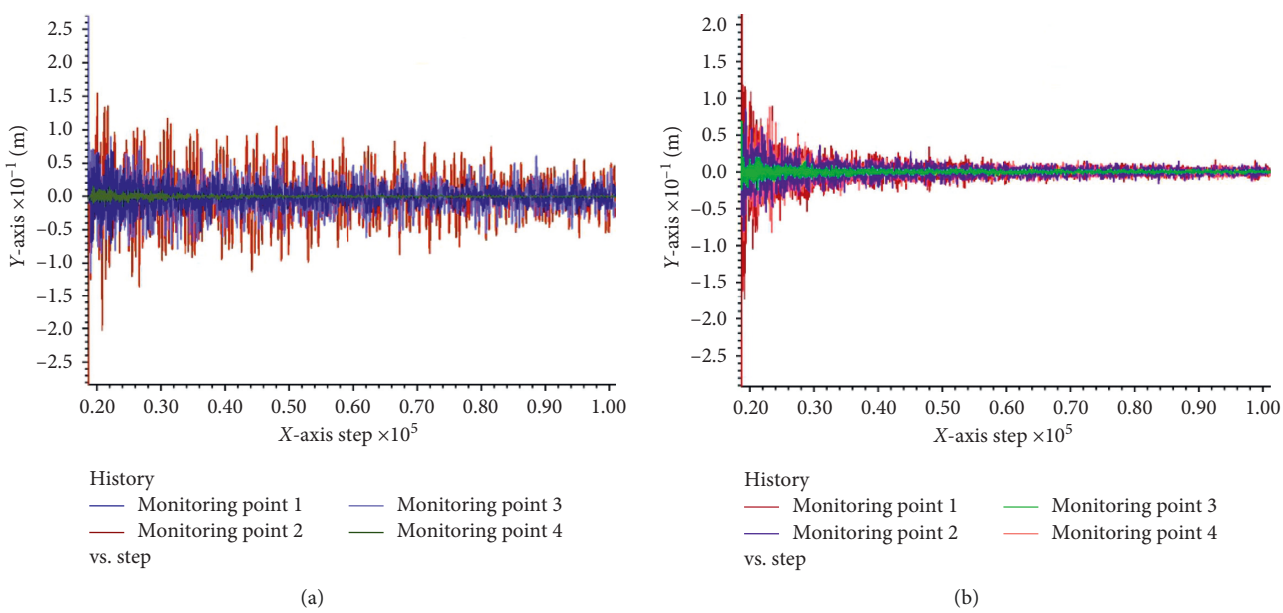

Figure 16: Velocity response diagram for six dynamic loads. (a) X-directional deformation velocity and (b) Z-directional deformation velocity.

strength of the anchors. Mining at the 103 working face results in an increase in deformation and support pressure requirements in the surrounding rock, and thus the working resistance of the cable anchors generally increases. The working resistance of the monitored bolt is generally 7–19 t, with an average of 11.05 t, which is 46.04% of its tensile strength. The working resistance of the cable anchors is generally 13–29 t, with an average of 17.14 t, which is 34.28% of its tensile strength.

The working resistance of bolts and cable anchors has not been fully exerted, mainly because the overall pre-tensioning force of the anchor support system is high and the support stiffness is large. This provides higher support resistance to surface breakage in the surrounding rocks over time, effectively restraining any shallow deformation that may lead to deeper breakage or failure. Importantly, this design improves the self-supporting ability of the rock, reducing deformation around the roadway. This reduction

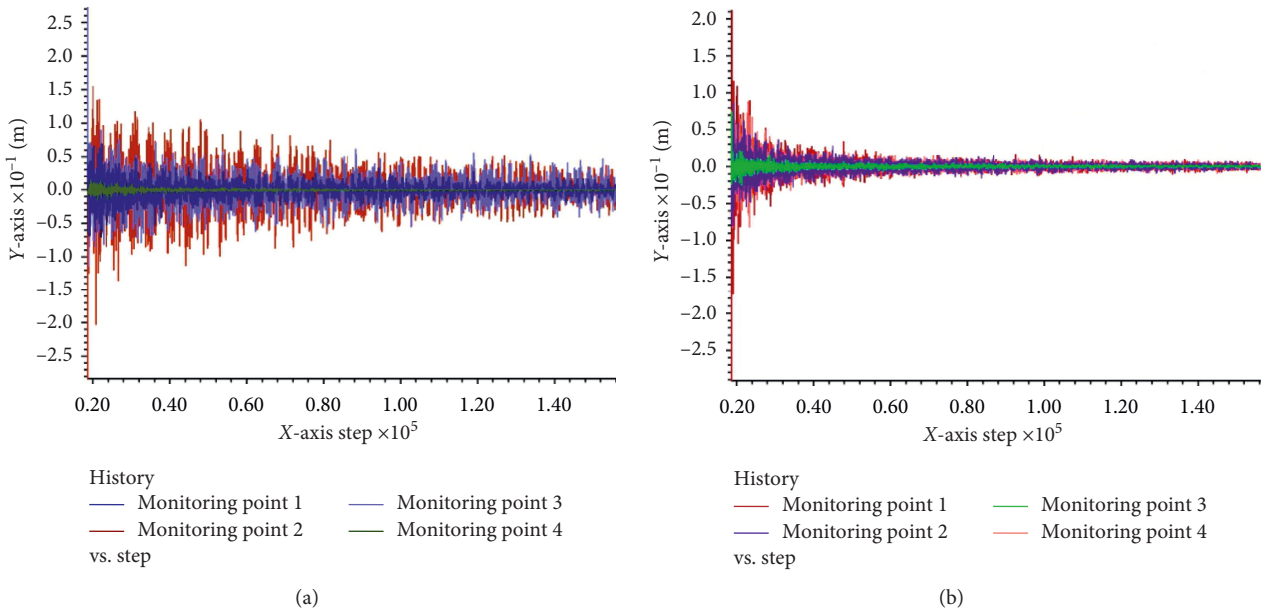

Figure 17: Velocity response diagram for ten dynamic loads. (a) X-directional deformation velocity and (b) Z-directional deformation velocity.

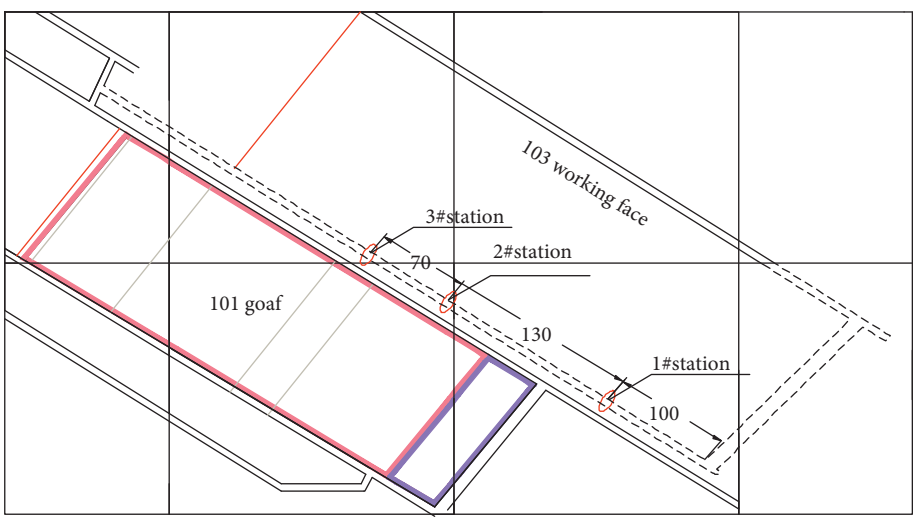

Figure 18: Schematic diagram showing the layout of stations #1, #2, and #3.

in deformation also provides an explanation for why the working resistance of the anchors is not fully exerted. Finally, the support strength of the cable anchor support system exceeds the support requirements of the gob-side entry (103 working face).

5.2.1. Monitoring Results and Analysis of Surrounding Rock Deformation. Figures 20 and 21 show the monitoring results of surrounding rock deformation during the whole process of driving along the gob-side entry, from roadway excavation to mining.

The monitoring results at the two stations show that roof-to-floor convergence is low. For example, at station #2, the convergence is 126 mm, with an approach rate of only 3.71% during the whole process from excavation to mining. The average subsidence at station #3 is only 70.5 mm. The average displacement of a small pillar side along the goaf is 109 mm, and the average displacement of the 103 solid coal side is 93 mm. The deformation of the side of the small pillar is relatively large, especially in the early stage of roadway excavation, and the deformation rate of the pillar is also relatively large. As the roadway excavation time increases, the deformation rate of the side of the small pillar gradually decreases. Although the roadway is influenced by the significant mining depth and current mining at the 101 working face, the convergence deformation in rock surrounding the roadway is very small, indicating that the current support

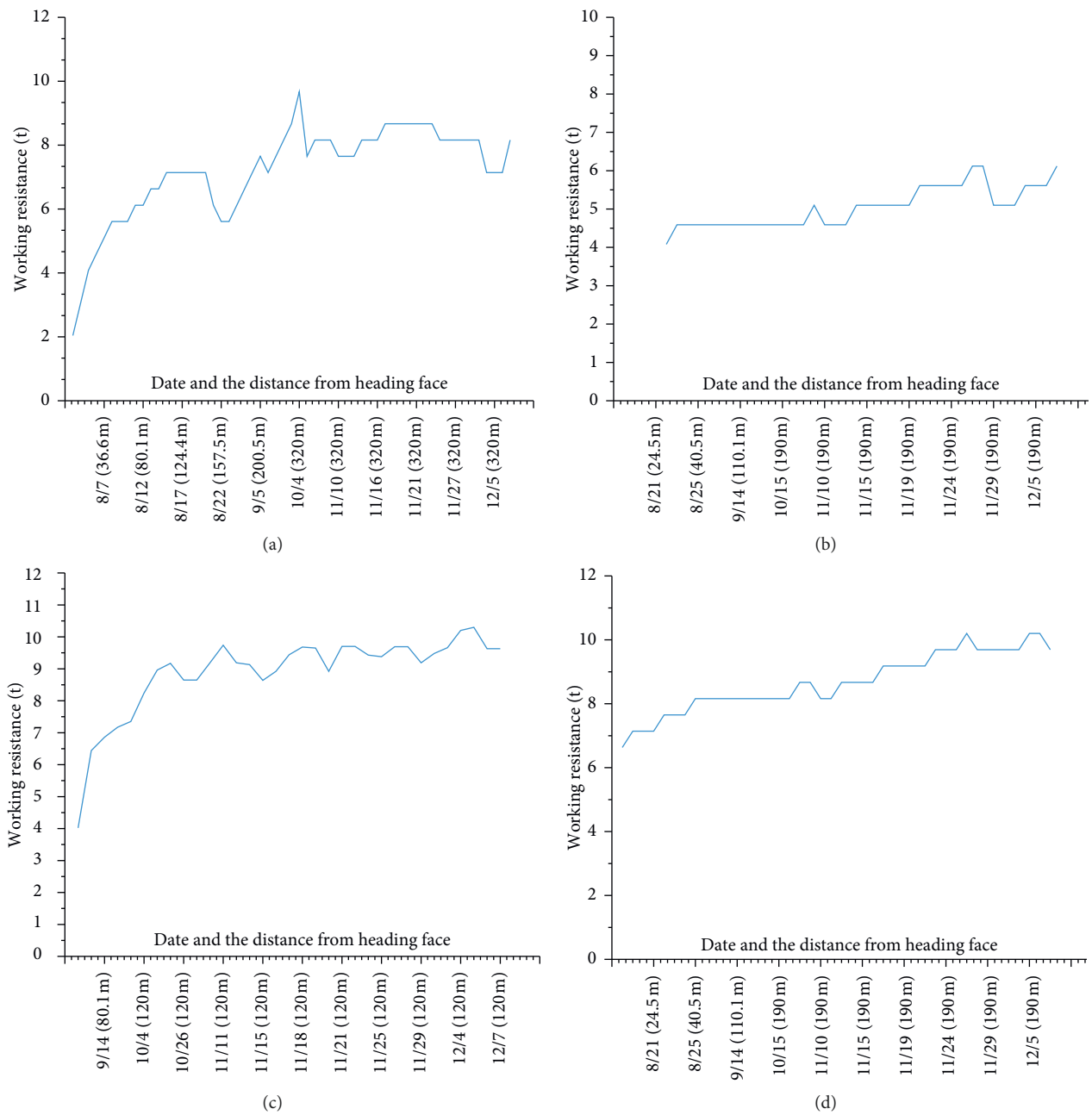

Figure 19: Continued.

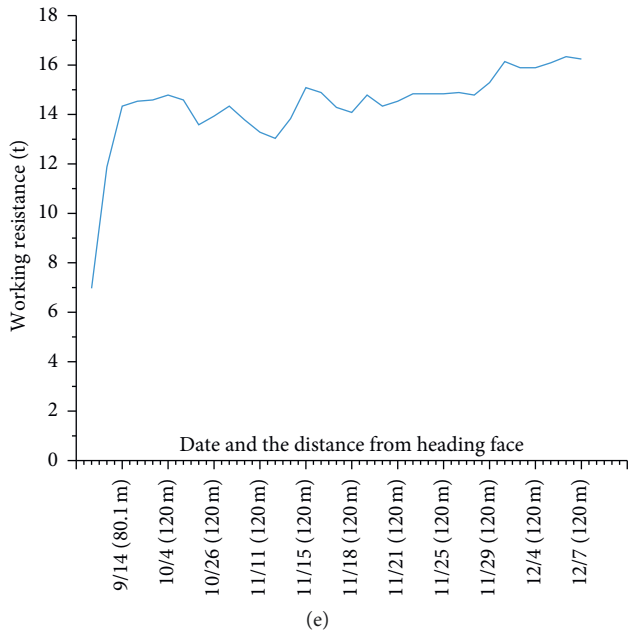

Figure 19: Curves of working resistance of bolts and cable anchors with increasing driving distance. (a) No. 1 bolt dynamometer at station #1, (b) No. 1 bolt dynamometer at station #2, (c) No. 1 bolt dynamometer at station #3, (d) No. 1 cable anchor dynamometer at station #2, and (e) No. 1 cable anchor dynamometer at station #3.

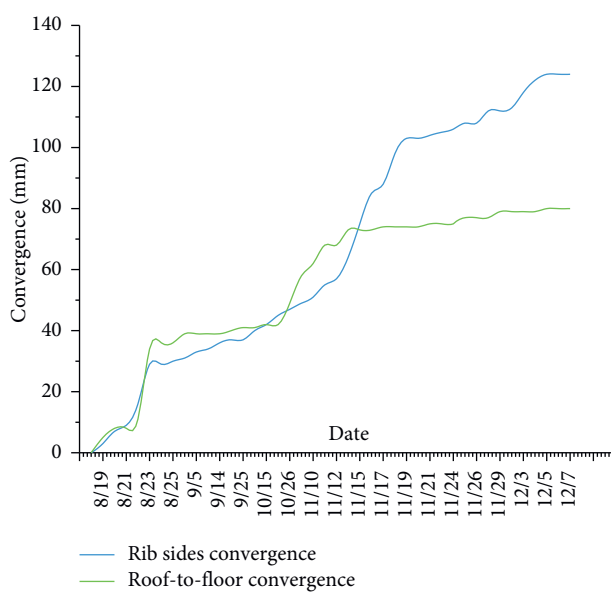

Figure 20: Convergence monitoring results of surrounding rock deformation at station #2.

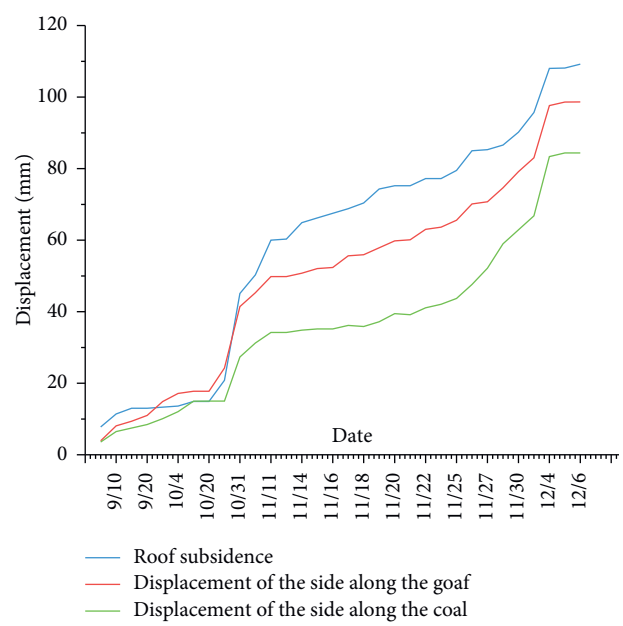

Figure 21: Displacement monitoring results of surrounding rock deformation at station #3.

parameters and support strength meet the roadway support requirements (return air way) along the gob of the 103 working face.

The pretensioning force of the anchors is relatively high as a whole, which increases support stiffness and strength. This not only provides time-sensitive support to the shallow surrounding rock of the roadway but also prevents deepening of breakage in the surrounding rock. The self-supporting ability of the surrounding rock is therefore improved as the range of loosening, deformation, and failure is effectively brought under control. The overall support strategy is therefore effective.

6. Conclusions

(1) Numerical simulation of the gob-side entry of the 103 working face, when subjected to multiple dynamic loads, shows that the plastic zone and displacement of the rock surrounding the roadway

gradually increase with increasing dynamic load. During the service period, the roadway will undergo many dynamic loads and it can be expected that the plastic zone will gradually increase, along with deterioration in the mechanical properties of the surrounding rock. The increasing trend does abate over time (Figure 4)

(2) The support strength and stiffness of the bolt support system should be increased to restrain the deterioration in mechanical properties of rock surrounding the gob-side entry. This will reduce the overall deformation and damage in the surrounding rock. As part of this strategy, yielding bolts (cable anchors) with large shrinkage should be adopted. Any unnecessary supporting loads should also be removed to prevent failure of cable anchors or rock failure under large loads

(3) Bolt support optimization design of the gob-side entry of the 103 working face was carried out with the concept of overall coupling to equalize ground pressure. This was based on the characteristics of the damage range and serious deformation in rock surrounding the gob-side entry under dynamic load. The optimized bolt support system has high support strength and stiffness even when the surrounding rock is allowed to deform and hence is a successful design

(4) In-field application and monitoring of the optimized support design show that significant pretensioning of bolts and cables can be effective, reaching 20.83% and 22.96% of their tensile strengths, respectively. During the whole process from excavation to mining, the average of roof-to-floor convergence of the roadway is 126 mm, and the average rib side convergence is 198.3 mm. The optimized support design therefore satisfies the support requirements of the rock surrounding the gob-side entry of the 103 working face, effectively reducing the potential loosening, deformation, and failure of the surrounding rock. Additionally, more research work needs to be done for understanding this issue

Data Availability

The data used to support the findings of this study are included within the article.

Conflicts of Interest

The authors declare no conflicts of interest.

Acknowledgments

The authors wish to acknowledge financial support from the National Key R&D Program of China (no. 2018YFC0604705), the National Natural Science Foundation of China (no. 51574156), and the Taishan Scholar Talent Team Support Plan for Advantaged and Unique Discipline Areas.

References

[1] H. X. Liu, J. B. Wang, J. Zhao, X. Wang, and D. M. Zhu, "Critical technical problems of deep mining and preliminary solutions," *Mining Research and Development*, vol. 38, no. 5, pp. 1–5, 2018.

[2] J. B. Bai, J. B. Zhao, J. Zhao, X. Wang, and M. D. Zhu, "Control mechanism and support technique about gateway driven along goaf in fully mechanized top coal caving face," *Journal of China Coal Society*, vol. 25, no. 5, pp. 478–481, 2000.

[3] D. C. Wang, Q. Wang, S. C. Li et al., "Mechanism of rock deformation and failure and its control technology of roadway driving along next goaf in fully mechanized top coal caving face of deep mines," *Journal of Mining and Safety Engineering*, vol. 31, no. 5, pp. 665–672, 2014.

[4] T. T. Bu, J. G. Ning, J. Wang, and W. M. Zhang, "Study on reasonable size of coal pillar in fully-mechanized gob-side entry driving of thick coal sea," *Journal of Shandong University (Natural Science)*, vol. 36, no. 6, pp. 109–116, 2017.

[5] J. Hu, M. He, J. Wang, Z. Ma, Y. Wang, and X. Zhang, "Key parameters of roof cutting of gob-side entry retaining in a deep inclined thick coal seam with hard roof," *Energies*, vol. 12, no. 5, p. 934, 2019.

[6] L. M. Liu, J. P. Sun, W. Sun, B. Fu, and X. Yan, "Research and application of balanced support design method for fully-mechanized gobside entry driving with opposite mining direction," *Journal of Shandong University (Natural Science)*, vol. 36, no. 6, pp. 24–31, 2017.

[7] Y. L. Tan, Q. Ma, Z. H. Zhao et al., "Cooperative bearing behaviors of roadside support and surrounding rocks along gob-side," *Geomechanics and Engineering*, vol. 18, no. 4, pp. 439–448, 2019.

[8] Q. Ma, Y. L. Tan, Z. H. Zhao, Q. Xu, J. Wang, and K. Ding, "Roadside support schemes numerical simulation and field monitoring of gob-side entry retaining in soft floor and hard roof," *Arabian Journal of Geosciences*, vol. 11, no. 18, p. 563, 2018.

[9] M. Tadeusz, P. Małkowski, and Z. Niedbalski, "Rock mass movements around development workings in various density of standing-and-roof-bolting support," *Journal of Coal Science and Engineering (China)*, vol. 14, no. 3, pp. 356–360, 2008.

[10] Q. X. Qi, S. B. Chen, H. X. Wang, D. B. Mao, and Y. X. Wang, "Study on the relations among coal bump, rockburst and mining tremor with numerical simulation," *Chinese Journal of Rock Mechanics and Engineering*, vol. 22, no. 11, pp. 1852–1858, 2003.

[11] N. G. W. Cook, "The basic mechanics of rockburst," *Journal of the Southern African Institute of Mining and Metallurgy*, vol. 64, no. 3, pp. 71–81, 1963.

[12] C. A. Tang, *Catastrophe in the Process of Rock Fractur*, China Coal Industry Publishing House, Beijing China, 1993.

[13] Y. S. Zhang and M. T. Zhang, "Analysis of physical process of rockburst by catastrophe theory," *Journal of Fuxin Institute of Mining*, vol. 11, no. 1, pp. 12–18, 1992.

[14] H. He, L. Dou, S. Gong, L. Wang, M. Gao, and X. Zhang, "Mechanism of rockburst prevention and supporting control technology in roadways," *Journal of Mining and Safety Engineering*, vol. 27, pp. 40–44, 2010.

[15] W. J. Ju, "Energy checking design method of roadway with rock-burst danger," *Coal Mining Technology*, vol. 16, no. 3, pp. 81–83, 2011.

[16] A. Y. Cao, J. Fan, Z. L. Mou, and X. Q. Guo, "Burst failure effect of mining-induced tremor on roadway surrounding rock," *Journal of China Coal Society*, vol. 35, no. 12, pp. 2006–2010, 2010.

[17] R. Yang, Q. Li, Q. Li, and X. Zhu, "Assessment of bearing capacity and stiffness in new steel sets used for roadway support in coal mines," *Energies*, vol. 10, no. 10, p. 1581, 2017.
[18] J. J. Cui, "Study on deformation and failure mechanism and control technology of deeply gob-side entry driving," *Coal Science and Technology*, vol. 45, no. 7, pp. 12–17, 2017.
[19] J. B. Ma, J. Ma, S. Wang, and L. Deng, "Optimization of supporting parameters for deep coal roadway considering repeated impact dynamic load," *Safety in Coal Mines*, vol. 48, no. 7, pp. 212–215, 2017.
[20] W. Li, N. Yang, Y. Mei, Y. Zhang, L. Wang, and H. Ma, "Experimental investigation of the compression-bending property of the casing joints in a concrete filled steel tubular supporting arch for tunnel engineering," *Tunnelling and Underground Space Technology*, vol. 96, p. 103184, 2020.
[21] P. Wang, L. S. Jiang, P. Q. Zheng, G. P. Qin, and C. Zhang, "Inducing mode analysis of rock burst in fault-affected zone with a hard–thick stratum occurrence," *Environmental Earth Science*, vol. 78, no. 15, p. 467, 2019.
[22] L. S. Jiang, P. Wang, P. Q. Zheng, H. J. Luan, and C. Zhang, "Influence of different advancing directions on mining effect caused by a fault," *Advances in Civil Engineering*, vol. 2019, Article ID 7306850, 10 pages, 2019.
[23] Y. J. Yang, H. Q. Duan, L. Y. Xing, S. Ning, and J. K. Lv, "Fatigue characteristics of limestone under triaxial compression with cyclic loading," *Advances in Civil Engineering*, vol. 2018, Article ID 8681529, 12 pages, 2018.
[24] Y. J. Yang, L. Y. Xing, H. Q. Duan, L. Den, and Y. C. Xue, "Fatigue damage evolution of coal under cyclic loading," *Arabian Journal of Geosciences*, vol. 11, no. 18, p. 560, 2018.
[25] C. J. Lian, W. Y. Xu, Y. J. Wang, and Z. H. Wang, "Numerical simulation of entry performance supported by a new high strength and high pretension yield," *Rock and Soil Mechanics*, vol. 31, no. 7, pp. 2329–2335, 2010.
[26] J. D. Wang, Y. J. Wang, B. Z. Zhang, and L. L. Zhao, "Application of integral coupling high-level yielding equal pressure support in Honghui no. 4 mine," *China Coal*, vol. 39, no. 8, pp. 63–67, 2013.
[27] Z. Niedbalski, P. Małkowski, and T. Majcherczyk, "Monitoring of stand-and-roof-bolting support-design optimization," *Acta Geodynamica et Geomaterialia*, vol. 10, no. 2, pp. 215–226, 2013.